Available online at www.sciencedirect.com

ScienceDirect

Geochimica et Cosmochimica Acta 157 (2015) 213–227

Geochimica et Cosmochimica Acta

www.elsevier.com/locate/gca

Laboratory calibration of the calcium carbonate clumped isotope thermometer in the 25–250 °C temperature range

Tobias Kluge [a,*,1], Cédric M. John [a,2], Anne-Lise Jourdan [a], Simon Davis [a], John Crawshaw [a,b]

[a] Department of Earth Science and Engineering and Qatar Carbonate and Carbon Storage Research Centre (QCCSRC), Imperial College London, Prince Consort Road, London SW7 2AZ, UK

[b] Department of Chemical Engineering and Qatar Carbonate and Carbon Storage Research Centre (QCCSRC), Imperial College London, Prince Consort Road, London SW7 2AZ, UK

Received 6 June 2014; accepted in revised form 20 February 2015; available online 27 February 2015

Abstract

Many fields of Earth sciences benefit from the knowledge of mineral formation temperatures. For example, carbonates are extensively used for reconstruction of the Earth's past climatic variations by determining ocean, lake, and soil paleotemperatures. Furthermore, diagenetic minerals and their formation or alteration temperature may provide information about the burial history of important geological units and can have practical applications, for instance, for reconstructing the geochemical and thermal histories of hydrocarbon reservoirs.

Carbonate clumped isotope thermometry is a relatively new technique that can provide the formation temperature of carbonate minerals without requiring *a priori* knowledge of the isotopic composition of the initial solution. It is based on the temperature-dependent abundance of the rare ^{13}C–^{18}O bonds in carbonate minerals, specified as a Δ_{47} value. The clumped isotope thermometer has been calibrated experimentally from 1 °C to 70 °C. However, higher temperatures that are relevant to geological processes have so far not been directly calibrated in the laboratory.

In order to close this calibration gap and to provide a robust basis for the application of clumped isotopes to high-temperature geological processes we precipitated $CaCO_3$ (mainly calcite) in the laboratory between 23 and 250 °C. We used two different precipitation techniques: first, minerals were precipitated from a $CaCO_3$ supersaturated solution at atmospheric pressure (23–91 °C), and, second, from a solution resulting from the mixing of $CaCl_2$ and $NaHCO_3$ in a pressurized reaction vessel at a pressure of up to 80 bar (25–250 °C).

The calibration lines of both experimental approaches overlap and agree in the slopes with theoretical estimates and with other calibration experiments in which carbonates were reacted with phosphoric acid at temperatures above 70 °C. Our study suggests a universal Δ_{47}-T calibration (T in K, Δ_{47} in ‰):

$$\Delta_{47} = 0.98(\pm 0.01) \cdot (-3.407 \cdot 10^9/T^4 + 2.365 \cdot 10^7/T^3 - 2.607 \cdot 10^3/T^2 - 5.880/T) + 0.293(\pm 0.004)$$

This new Δ_{47}-T calibration (given in the absolute reference frame), that extends the experimentally calibrated temperature range for clumped isotopes to 250 °C, can be applied to carbonates that grew at intermediate temperatures (20–250 °C).

* Corresponding author at: Department of Earth Science and Engineering and Qatar Carbonate and Carbon Storage Research Centre, Imperial College London, Prince Consort Road, SW7 2BP London, UK.

E-mail addresses: tobias.kluge@iup.uni-heidelberg.de (T. Kluge), cedric.john@imperial.ac.uk (C.M. John).

[1] Institut für Umweltphysik, Universität Heidelberg, Im Neuenheimer Feld 229, 69120 Heidelberg, Germany. Tel.: +49 6221 54 6511; fax: +49 6221 54 6405.

[2] Tel.: +44 20759 46461.

http://dx.doi.org/10.1016/j.gca.2015.02.028

0016-7037/

1. INTRODUCTION

The carbonate clumped isotope thermometer has rapidly evolved as a new and highly promising tool in Earth sciences (see reviews of Eiler, 2007, 2011, 2013; Affek, 2012). Its application recently turned toward geological applications that use carbonates precipitated during burial of sedimentary sequences. In this context carbonate clumped isotopes can give insights into the evolution of subsurface fluid flow (Budd et al., 2013), elucidate the origin of debated carbonate sequences (Bristow et al., 2011), constrain temperature and fluids related to faults (Swanson et al., 2012), and determine the formation temperature of carbonate phases (Ferry et al., 2011; Huntington et al., 2011; Loyd et al., 2012; Price and Eiler, 2013; Dale et al., 2014). Beyond these applications carbonate clumped isotopes can provide valuable information for the geochemical characterization of hydrocarbon reservoirs (e.g., Bergman et al., 2010; Huntington et al., 2011) and mineral deposits (Price and Eiler, 2013).

Despite the wide range of promising applications of the clumped isotope proxy in the subsurface, the exact clumped isotope temperature relationship has not been determined experimentally in the relevant temperature field for applications to the shallow lithosphere and anchizone (i.e., temperatures up to 250 °C). Experimental and empirical clumped isotope Δ_{47}-T relationships are readily available for paleoclimate research on carbonates encompassing typical Earth surface temperatures (Ghosh et al., 2006; Dennis and Schrag, 2010; Tripati et al., 2010; Eagle et al., 2013; Grauel et al., 2013; Henkes et al., 2013; Zaarur et al., 2013). For higher temperatures either the theoretical calibration of Guo et al. (2009) is used or a linear extrapolation of the empirical low-temperature relationship of Ghosh et al. (2006; 1–50 °C) is applied. The difference between these calibrations can cause substantial deviations between reconstructed mineral formation temperatures. For example, a clumped isotope Δ_{47} value of 0.3‰ (detailed explanation in Section 3) corresponds to a temperature of 183 °C using the extrapolation of the calibration of Ghosh et al. (2006) in the reference frame of Dennis et al. (2011), but to ~320 °C using the theoretical model of Guo et al. (2009). This vast difference could be explained by the inappropriate extrapolation of the low-temperature calibration of Ghosh et al. (2006), determined between 1 and 50 °C, to higher temperatures and uncertainties of its slope (Zaarur et al., 2013) that are enhanced beyond the experimental temperature range. Furthermore, it illustrates the need for experimental verification of the actual clumped isotope temperature relationship beyond Earth surface temperatures. This will reduce existing uncertainties and can be used as an important test for the theoretical assessment of the temperature relationship of carbonate clumped isotopes.

Passey and Henkes (2012) studied the solid-state resetting of clumped isotope values by equilibrating sets of spar calcite samples between 475 and 800 °C. Using these new data points as high-temperature constraints, their results suggest the clumped-isotope temperature relationship closely follows the theoretical result of Schauble et al. (2006) and Guo et al. (2009). However, a calibration gap still exists between 70 and 475 °C that needs to be addressed to establish applications of the clumped isotope thermometer to carbonates precipitated above 70 °C.

We precipitated a suite of carbonates under controlled conditions in the laboratory to assess the temperature dependence of the ^{13}C–^{18}O clumping in the gap between low- and high-temperature calibrations, spanning temperatures from 20 °C to 250 °C and aimed to significantly reduce the uncertainty in this temperature range. In order to ensure reproducibility and representativeness, carbonates were precipitated using two different methods. In the first setup, minerals precipitated from an isotopically equilibrated $CaCO_3$ solution at atmospheric pressure, whereas minerals in the second experiment were precipitated from a solution prepared by mixing equilibrated solutions of $CaCl_2$ and $NaHCO_3$ in a pressurized reaction vessel.

2. LABORATORY PRECIPITATION OF CARBONATES

The carbonate samples measured in this study were precipitated using two distinct techniques and were formed under controlled conditions (temperature, pressure) in the laboratory. One set of experiments was conducted at atmospheric pressure and involved temperatures of 23–91 °C. Minerals formed in this case from a slightly super-saturated $CaCO_3$ solution that was prepared by dissolving ~360 mg of pure $CaCO_3$ in 500 ml de-ionized water at 25 °C. The dissolved inorganic carbon was isotopically equilibrated with the bulk water at the respective experiment temperature after a filtration step in which un-dissolved components were removed. Carbonate formation was induced by controlled slow bubbling of CO_2 (details in the Supplementary Material). The experimental method is similar to that used by Ghosh et al. (2006) and Zaarur et al. (2013), but is different from the approach of Dennis and Schrag (2010) where passive degassing led to mineral formation. The second technique applied in our study used a pressurized reaction vessel in which $CaCO_3$ was precipitated at temperatures of up to 250 °C from a solution prepared by mixing a $CaCl_2$ and $NaHCO_3$ solution.

Isotopic equilibration of the dissolved inorganic carbon (DIC) with the bulk water in both mineral growth experiments was achieved by storing the solution at the experimental temperature for a sufficiently long time period (between 2 h at $\geqslant$90 °C and >15 h at 25 °C) and preventing mineral formation during this time. The equilibration time is dependent on solution temperature and pH and was chosen based on the experiments of Beck et al. (2005) and Uchikawa and Zeebe (2012).

2.1. Carbonate precipitation from mixing a $NaHCO_3$ and $CaCl_2$ solution

An experimental procedure was developed to enable carbonate formation at controlled conditions and temperatures of up to 250 °C. The apparatus (Fig. 1; details in Supplementary Material) consists of a pressurized reaction vessel in which two fluids can be injected separately (here:

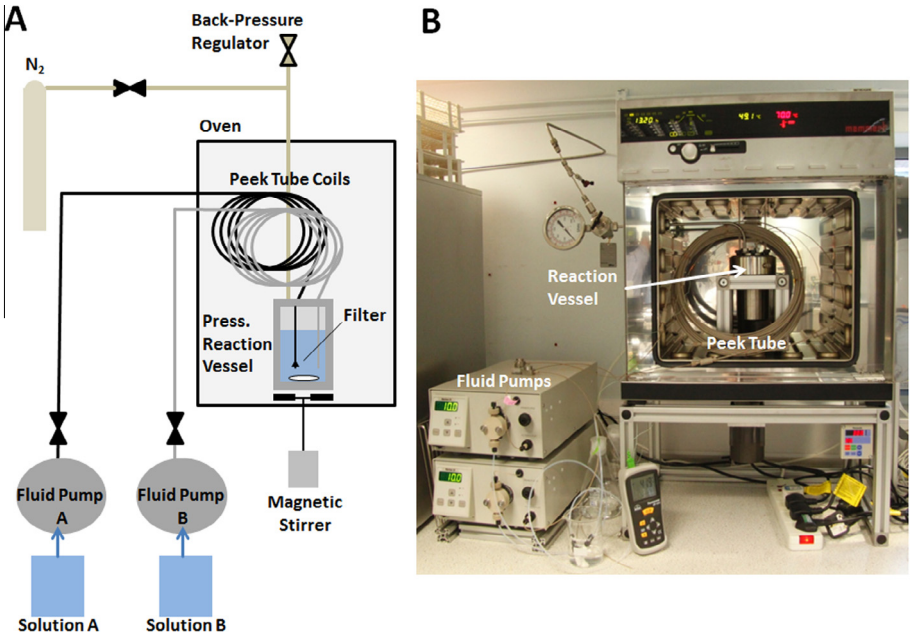

Fig. 1. Experimental setup used to precipitate carbonate minerals at high temperatures up to 250 °C (scheme: A, photo: B). Peristaltic pumps inject two diluted solutions via two different tubes (containing $NaHCO_3$ and $CaCl_2$, respectively) into the pressurized reaction vessel (inside oven). The solutions are kept at experiment temperature in PEEK tubes (0.03″ inner diameter; Kinesis Ltd.) for isotopic equilibration before injection into the pressurized reaction vessel (see Section 3). The solution inside the pressurized reaction vessel is continuously stirred during the experiment. Details about the pressurized reaction vessel are given in the Supplementary Material.

0.10 molal $CaCl_2$ and 0.18 molal $NaHCO_3$ solutions) using two peristaltic pumps. These fluids were isotopically equilibrated before injection into the pressurized reaction vessel by storing them for 3 h (at an oven temperature of 250 °C) to 50 h (oven temperature of ~25 °C) in separate PEEK tube coils (50 ml volume each, 1/8' outer diameter) in a temperature-controlled oven (Memmert, UNE 200). The pressure in the reaction vessel was adjusted using N_2 tank gas according to the experiment temperature to avoid boiling of the mixed fluids (1–80 bar). After isotope equilibration, the two fluids were displaced into the reactor by pumping additional liquid into the coils at a rate of few ml/min. The volume of the displacing fluid was limited to <50 ml such that only pre-equilibrated fluid entered the reactor. The solution in the pressurized reaction vessel was continuously stirred in order to ensure a homogeneous fluid composition during mineral formation. At the end of each experiment (after 2–12 days) the water was either directly released from the pressurized reaction vessel through a fine filter (0.5 µm) at the end of the injection tubes using the pressure in the experimental setup or after a cooling period of <2 h to prevent fluid boiling during pressure reduction (average cooling rates: 0.02–0.06 Ks^{-1}). The minerals were collected by flushing the reaction vessel with de-ionized water and subsequent filtration of this solution with a double layer of Whatman™ filter paper (grade 1). The recovered $CaCO_3$ crystals were air-dried at room temperature. Related experiment details are summarized in Table 3. Newly formed $CaCO_3$ crystals were inspected microscopically and via X-ray diffraction (see Section 3.4.) before analysing them for clumped isotopes.

3. ANALYTICAL METHODS

3.1. Carbonate clumped isotopes

Carbonate clumped isotopes refer to $CaCO_3$ molecules that include two or more rare isotopes such as ^{13}C and ^{18}O. The abundance of these multiply-substituted isotopologues is governed by thermodynamic parameters (Wang et al., 2004) that depend on the rotational and vibrational frequencies of the relevant bonds. For CO_2 gas, produced from acid digestion of carbonates, the abundance of ^{13}C–^{18}O bonds carries information about the carbonate formation temperature. The abundance of ^{13}C–^{18}O bonds in the analyzed CO_2 is evaluated with regard to its stochastic distribution at high temperatures (>1000 °C) and specified as Δ_{47} value (Eiler and Schauble, 2004; Affek and Eiler, 2006):

$$\Delta_{47} = \left[\frac{R^{47}}{2R^{13}\cdot R^{18} + 2R^{17}\cdot R^{18} + R^{13}\cdot (R^{17})^2} - \frac{R^{46}}{2R^{18} + 2R^{13}\cdot R^{17} + (R^{17})^2} - \frac{R^{45}}{R^{13} + 2R^{17}} + 1 \right] \cdot 1000 \quad (1)$$

The Δ_{47} value is calculated from the measured ratios (R^i) of masses 45, 46 and 47 to mass 44 and by calculating R^{13} ($^{13}C/^{12}C$) and R^{18} ($^{18}O/^{16}O$) from R^{45} and R^{46} assuming random distribution. R^{17} is calculated from R^{18} assuming a mass-dependent relationship between ^{18}O and ^{17}O.

The Δ_{47} value under conditions of isotopic equilibrium increases with decreasing temperature (Wang et al., 2004),

Table 1
Experimental and theoretical Δ_{47}-temperature calibrations of $CaCO_3$ (mainly calcite). Experimental calibrations are shown in the absolute reference frame of Dennis et al. (2011). The results of this study are combined with data of Dennis and Schrag (2010), Passey and Henkes (2012) and Tang et al. (2014). A compilation of Δ_{47} data acquired by acid digestion at 90 °C is also given without acid fractionation correction (marked by an asterisk).

Δ_{47}-T relationship (T in K, Δ_{47} in ‰)	Calibration range	Precipitation method/material	Acid digestion T (°C)	References
Experimental methods, inorganic precipitates				
$0.636\ (\pm0.049)\cdot10^5/T^2 - 0.005\ (\pm0.052)$	1–50 °C	From supersaturated $Ca(HCO_3)_2$	25 °C, over night	Ghosh et al. (2006), Dennis et al. (2011)
$0.362\ (\pm0.018)\cdot10^5/T^2 + 0.292\ (\pm0.019)$	7.5–77 °C	Mixing $CaCl_2$ and $NaHCO_3$	90 °C, 10 min	Dennis and Schrag (2010), Dennis et al. (2011)
$0.555\ (\pm0.027)\cdot10^5/T^2 + 0.078\ (\pm0.030)$	5–65 °C	From supersaturated $Ca(HCO_3)_2$	25 °C, over night	Zaarur et al. (2013)
Experimental methods, re-ordering				
$-3.407\cdot10^9/T^4 + 2.365\cdot10^7/T^3 - 2.607\cdot10^3/T^2 - 5.880/T + 0.280$	475–800 °C	Re-ordering of $CaCO_3$	90 °C	Passey and Henkes (2012)
Theoretical studies				
$-3.330\cdot10^9/T^4 + 2.324\cdot10^7/T^3 - 2.913\cdot10^3/T^2 - 5.540/T + 0.233$	260–1500 K	Theory	–	Guo et al. (2009) (based on Schauble et al., 2006)
$0.40464\cdot10^5/T^2 + 0.181$	0–250 °C Linear fit	Theory	–	Data from Guo et al. (2009) (Only low temperatures)
Experimental results, this study				
$0.380\ (\pm0.07)\cdot10^5/T^2 + 0.259\ (\pm0.006)$	23–250 °C	From supersaturated $Ca(HCO_3)_2$/mixing $CaCl_2$ and $NaHCO_3$	70 °C/90 °C	This study, linear fit vs. $1/T^2$
$0.98^*(-3.407\cdot10^9/T^4 + 2.365\cdot10^7/T^3 - 2.607\cdot10^3/T^2 - 5.880/T) + 0.293$	7.5–250 °C, 475–800 °C	Inorganic lab. minerals, reordering experiments	70–100 °C	This study combined with Dennis and Schrag (2010), Passey and Henkes (2012) and Tang et al. (2014) Two-parameter fit to theory of Schauble et al. (2006)
$0.397\ (\pm0.003)\cdot10^5/T^2 + 0.248\ (\pm0.002)$	7.5–250 °C, 475–800 °C	Inorganic lab. minerals, reordering experiments	70–100 °C	Combined as above, linear fit vs. $1/T^2$
$0.405\ (\pm0.004)\cdot10^5/T^2 + 0.167\ (\pm0.002)^*$	7.5–250 °C, 475–800 °C	Inorganic lab. minerals, reordering experiments	90 °C	Combined as above, linear fit vs. $1/T^2$ Not acid corrected to 25 °C reactions

is negligibly dependent on the bulk $\delta^{18}O$ and $\delta^{13}C$ composition (Cao and Liu, 2012) and independent of the parent fluid composition, making it an ideal paleotemperature proxy. Previously published experimental Δ_{47}-T relationships together with the applied experimental procedures are summarized in Table 1.

3.2. Sample treatment for carbonate clumped isotope analysis

Carbonate samples weighing 5–8 mg were inserted into the inlet part of a custom-built reaction vessel that allows sample storage separate from the 105% phosphoric acid at its bottom (~2 ml per sample). The reaction vessel, containing the carbonate sample and ortho-phosphoric acid, was evacuated for 30 min on the manual extraction line and typically reached pressures of 10^{-1}–10^{-2} mbar before the acid digestion was initiated. The baseline pressure of the line is 10^{-3}–10^{-4} mbar. The slightly higher pressure at the inlet part with attached reaction vessel is due to degassing of residual atmospheric gases from the phosphoric acid. The $CaCO_3$ aliquots were generally reacted with ortho-phosphoric acid for 10 min at 90 °C in a stirred reaction vessel with the evolving CO_2 being continuously collected. A few samples were reacted at 70 °C for 15 min (Table 2). The reaction vessel was completely cleaned of any residue and acid after each phosphoric acid reaction and filled with new acid for the next sample. No common acid bath was used for this procedure.

The reactant CO_2 was cleaned using a procedure initially described by Dennis and Schrag (2010). In brief, the evolved CO_2 was continuously trapped during the phosphoric acid reaction by freezing it in a liquid nitrogen-cooled trap. Volatile gases were then cryo-distilled from this trap at liquid nitrogen temperature. Subsequently, water was separated from the remaining gas using a dry-ice ethanol cooled glass trap. The dry CO_2 gas is then passively passed through another trap filled with silver wool and an additional trap densely packed with Porapak Q (filled length: 13 cm, inner diameter: ~8 mm) held at −35 °C. The efficiency of the Porapak trap was successfully tested with initially contaminated samples (elevated mass 48 and 49 mass spectrometer signals if run without cleaning). The clean CO_2

Table 2
Experimental conditions during laboratory carbonate precipitation following the methods of McCrea (1950) and O'Neil et al. (1969) ('water bath', see Section 2). The mineralogy was determined by X-ray diffraction measurements. The uncertainty in the mineral phase quantification is about 3%.

Experiment No.	$CaCO_{3,dissolved}$ (g/l)	T (°C)	Added salts (g/l)	Equilibration time (h)	Precipitation time (h)	Mineralogy
Water bath						
1	0.74	23.5 ± 0.5	–	17	147	Calcite
2	1.00	25.7 ± 0.5	–	15	72	Calcite
3	0.70	37.5 ± 0.5	–	17	100	Calcite
4	0.60	49.6 ± 0.5	–	15	30	Calcite (55%), aragonite (45%)
5	0.74	49.6 ± 0.5	–	17	195	Calcite
6	0.60	69.9 ± 0.5	–	17	44	Calcite (57%) aragonite (43%)
7	0.76	69.9 ± 0.5	–	18	25	Calcite (90%) aragonite (10%)
8	0.70	79.9 ± 0.5	–	3	~20	Calcite (78%) aragonite (22%)
9	0.78	91.0 ± 0.5	–	2	22	Calcite (72%) aragonite (28%)
10	0.74	91.0 ± 0.5	–	3	138	Aragonite (83%), calcite (17%)
NaCl added						
NA-1	0.68	23.5 ± 0.5	250	23	451	Vaterite
NA-2	0.60	25.7 ± 0.5	300	15	168	Calcite, aragonite*
NA-3	0.70	37.5 ± 0.5	260	21	72	Vaterite (95%), calcite (5%)
NA-4	0.74	37.5 ± 0.5	244	14	341	Vaterite (>95%), rest: calcite
NA-5	0.70	49.6 ± 0.5	375	16	143	Vaterite
NA-6	0.80	49.6 ± 0.5	262	17	573	Vaterite
NA-7	0.70	69.9 ± 0.5	325	3	69	Vaterite
NA-8	0.78	79.9 ± 0.5	280	3	47	Calcite (49%), aragonite (24%), vaterite (27%)
NA-9	0.70	91.0 ± 0.5	260	3	42	Vaterite (94%), aragonite (6%), calcite (<1%)

* Checked via microscopy only.

gas was then transferred to the dual inlet system of the mass spectrometer for analysis directly after purification.

3.3. Mass spectrometric analysis and data evaluation

Mass spectrometric analyses were performed on one of two separate isotope ratio mass spectrometers (MAT 253, Thermo Scientific) at the Qatar Stable Isotope Lab at Imperial College. The analysis protocol followed procedures described by Huntington et al. (2009) and Dennis et al. (2011) comprising measurements that consisted of 8 acquisitions with 7 cycles per acquisition and an integration time of 26 s. Each cycle included a peak center, background measurements and an automatic bellows pressure adjustment aimed at a 15 V signal at mass 44. The sample gas was measured against an Oztech reference gas standard ($\delta^{13}C = -3.63‰$ VPDB, $\delta^{18}O = -15.79‰$ VPDB and $\delta^{13}C = -3.62‰$ VPDB, $\delta^{18}O = -15.73‰$ VPDB for the two mass spectrometer, respectively). Heated gases (1000 °C), water-equilibrated gases (25 °C, 50 °C, 80 °C), a Carrara Marble ($\Delta_{47,abs} = 0.312‰$ at 90 °C) and an inter-laboratory carbonate standard ('ETH3', $\Delta_{47,abs} = 0.634‰$ at 90 °C) were measured regularly to transfer the measured values into the absolute reference frame (Dennis et al., 2011). The values of 'ETH3' and in-house Carrara Marble were measured against water-equilibrated CO_2 gases before being used as standards. The inter-laboratory standard 'ETH3' was provided by Stefano Bernasconi from the ETH Zurich. All sample and standard data are given in the Supplementary Material together with heated gases and transfer functions.

Contamination was monitored using the mass 48 and mass 49 signals. Sample measurements were rejected based on elevated 48 and 49 signals. A deviation from the δ_{48}–Δ_{48} relationship of clean standards of more than 2‰ (Dale et al., 2014) and mass 49 values above 0.2 were used as threshold (mass 49 value = 10,000 * [(49 signal/44 signal)$_{sample}$ − (49 signal/44 signal)$_{standard}$]). Δ_{47} values were first linearity-corrected using heated gas data (Huntington et al., 2009) and subsequently transferred into the reference frame of Dennis et al. (2011). For comparability with existing calibration lines we applied a phosphoric acid correction of 0.069‰ at 90 °C (0.052‰ at 70 °C) for calcite to the Δ_{47} values in the absolute reference frame following the theoretical considerations of Guo et al. (2009). The acid fractionation correction at 90 °C relative to a 25 °C phosphoric acid reaction varies between 0.07‰ and 0.09‰ in different experimental studies (Passey and Henkes, 2012; Henkes et al., 2013; Wacker et al., 2013; Tang et al., 2014). The theoretical value of Guo et al. (2009) is consistent with a recent empirical evaluation of the phosphoric acid reaction of calcite and aragonite (e.g., Wacker et al., 2013) and was therefore chosen in the absence of an in-house assessment of the acid fractionation value. We use an acid fractionation factor of 0.069‰ at 90 °C and of 0.052‰ at 70 °C for all measured calcium-carbonate polymorphs to simplify the evaluation and interpretation.

Carbonate $\delta^{18}O$ values were calculated using the acid fractionation factors of Kim and O'Neil (1997) with the correction of Böhm et al. (2000) for calcite and the acid fractionation factors of Kim et al. (2007) for aragonite. Mixtures of calcite and aragonite crystals are

Table 3
Experimental conditions during laboratory carbonate precipitation initiated by mixing of a $CaCl_2$ and $NaHCO_3$ solution ('reaction vessel', see Section 2). The mineralogy was determined by X-ray diffraction measurements. The uncertainty in the mineral phase quantification is about 3%.

Experiment No.	$NaHCO_3$ (molal)	$CaCl_2$ (molal)	T (°C)	Pressure (bar)	Equilibration time (h)	Precipitation time (h)	Mineralogy
Reaction vessel							
R-1	0.17	0.10	25 ± 2	1	50.5	281.5	Calcite
R-2	0.18	0.10	50 ± 2	1	67	221	Calcite
R-3	0.18	0.10	80 ± 2	1	24	144.75	Calcite (21%), aragonite (79%)
R-4	0.18	0.10	100 ± 2	20	4	66.25	Calcite
R-5	0.18	0.10	125 ± 2	20	6.25	113.5	Calcite
R-6	0.18	0.10	150 ± 2	28	4.6	44.5	Calcite
R-7	0.18	0.10	175 ± 2	28–34	3.5	59.5	Calcite
R-8	0.18	0.10	200 ± 2	28–36	4.25	47.5	Calcite
R-9	0.18	0.10	225 ± 2	60	7	142.5	Calcite
R-10	0.18	0.10	250 ± 2	80	3	41	Calcite

proportionally evaluated using the corresponding fractionation factors. The calcite fractionation factor was used for vaterite due to the lack of an accepted fractionation factor for vaterite. The studies of Tarutani et al. (1969) and Kim and O'Neil (1997) suggest an enrichment of vaterite relative to calcite of 0.5‰ and 0.6‰, respectively. We used the fractionation factor of Kim and O'Neil (1997) to calculate the solution $\delta^{18}O$ value from the measured $\delta^{18}O$ value of the calcite (or vaterite) fraction and the fractionation factor of Kim et al. (2007) for the aragonite fraction. The solution water $\delta^{18}O$ value was not measured on individual in-situ water aliquots.

The analytical uncertainties of the Δ_{47}, $\delta^{18}O$, and $\delta^{13}C$ measurements were added by Gaussian error propagation. We used the standard error of the mean in the case of replicate analysis and the standard deviation (SD) for single analyses (1σ SD: ~0.02‰ for Δ_{47}, 0.2‰ for $\delta^{18}O$, and 0.1‰ for $\delta^{13}C$).

3.4. X-ray diffraction (XRD) analysis

Minerals precipitated in the laboratory were examined for their crystallographic structure prior to the clumped isotope analysis. XRD measurements were performed at the National History Museum London using an Enraf Nonius FR 590 Powder Diffractometer with Cu Kα radiation (40 kV, 35 mA). Carbonate samples were placed as a thin layer on a sapphire substrate and measured in a fixed beam-sample-detector geometry with a 5° incidence angle between X-ray beam and sample. Signals are recorded by an INEL 120° position-sensitive detector. Analysis times varied between 10 and 90 min depending on the counting statistics and step size. The signals were evaluated by comparing measured spectra with a mineral data base using the program X'Pert Highscore (PANalytical B.V., 2009). Peak positions were calibrated with two standards (silver behenate and quartz). Pure calcite and aragonite standards were measured for phase quantification. The aragonite and calcite phase fractions were determined via comparison with the pure standards using an automated routine of the X'Pert Highscore software.

4. RESULTS

XRD analyses confirmed all minerals to be polymorphs of $CaCO_3$ (Tables 2 and 3). Mixing of $CaCl_2$ and $NaHCO_3$ solutions in the pressurized reaction vessel generally resulted in calcite, with one exception of dominantly aragonite at 80 °C (Table 3). Carbonate minerals formed from the $CaCO_3$ super-saturated solution as either pure calcite or primarily calcite with aragonite admixture. In a single experiment at 90 °C aragonite was the major carbonate phase (Table 2). Addition of NaCl (4–6.5 mol/l) resulted mostly in the precipitation of vaterite (Table 2).

The back-calculated solution water $\delta^{18}O$ values yield an average of -6.9 ± 0.9‰ for the water bath experiments (Table 4) and -2.5 ± 2.7‰ for solutions in the pressurized reaction vessel (Table 5). Disregarding two outliers, the high-temperature experiment in the pressurized reaction vessel results in a mean solution $\delta^{18}O$ value of -3.6 ± 1.3‰. The $\delta^{18}O_{water}$ value of the solution was back-calculated using the carbonate $\delta^{18}O$ value, the experiment temperature, and the fractionation factors corresponding to the precipitated mineral assemblage (see Section 3.3). The solution $\delta^{18}O$ was determined to check for potential kinetic effects that may occur during mineral precipitation. The de-ionized water is processed from local tap water supply that has an isotopic composition similar to ground and surface water in the London Metropolitan area of −6 to −7‰ (Darling et al., 2003). The calculated solution water $\delta^{18}O$ values of the water bath experiment are in agreement with the water source, whereas it is more positive for the pressurized reaction vessel. A trend toward positive $\delta^{18}O_{water}$ values with increasing reaction temperature is observed for the back-calculated solutions in the pressurized reaction vessel (Table 5).

$\delta^{13}C$ values were analyzed as part of the Δ_{47} measurement procedure (Tables 4 and 5). Variations in the carbonate $\delta^{13}C$ values of the water bath experiment are due to differences in the equilibration procedure. The solution was stored in a closed flask under a CO_2 atmosphere at low temperatures (≤50 °C) showing comparatively positive $\delta^{13}C$ values (on average −19.2‰), whereas CO_2 was actively bubbled through it at higher temperatures to

Table 4
Δ_{47}, $\delta^{18}O$, and $\delta^{13}C$ values of laboratory carbonate precipitates. $\delta^{18}O_{water}$ is the back-calculated solution isotope value based on the carbonate $\delta^{18}O$ value, the experimental temperature and the fractionation factors corresponding to the involved mineralogy (see Section 3.3). *n* indicates the number of replicate samples analysed. $\Delta_{47,uncorrected}$ gives the sample value without acid correction. Samples marked by an asterisk were acid digested at 70 °C (unmarked samples at 90 °C). Samples digested at 70 °C and 90 °C in different runs are disregarded in this column and marked by a '+'. Uncertainties for Δ_{47} measurements are given as 1 SE (1σ for a single analysis) and as 1σ standard deviation for $\delta^{18}O$, $\delta^{13}C$ and $\delta^{18}O_{water}$.

Experiment No.	*n* (-)	T (°C)	Δ_{47} (‰)	$\Delta_{47,uncorrected}$ (‰)	$\delta^{18}O$ (‰)	$\delta^{13}C$ (‰)	$\delta^{18}O_{water}$ (‰)
No salt added							
1	3	23.5 ± 0.5	0.691 ± 0.004	0.639*	−8.24 ± 0.08	−18.51 ± 0.04	−6.4 ± 0.1
2	3	25.7 ± 0.5	0.706 ± 0.010	0.654*	−8.40 ± 0.51	−17.05 ± 0.11	−6.1 ± 0.5
3	4	37.5 ± 0.5	0.670 ± 0.023	+	−12.38 ± 0.18	−20.61 ± 0.11	−7.8 ± 0.2
4	2	49.6 ± 0.5	0.625 ± 0.016	0.573*	−13.51 ± 0.28	−19.04 ± 0.01	−6.8 ± 0.3
5	3	49.6 ± 0.5	0.628 ± 0.013	0.559	−14.04 ± 0.11	−28.23 ± 0.10	−7.4 ± 0.1
6	2	69.9 ± 0.5	0.584 ± 0.020	0.532*	−15.43 ± 0.01	−19.42 ± 0.01	−5.6 ± 0.1
7	3	69.9 ± 0.5	0.577 ± 0.008	0.525*	−16.89 ± 0.11	−23.22 ± 0.12	−7.0 ± 0.2
8	6	79.9 ± 0.5	0.551 ± 0.013	+	−16.97 ± 0.06	−25.01 ± 0.07	−5.6 ± 0.1
9	3	91.0 ± 0.5	0.528 ± 0.007	0.476*	−18.84 ± 0.10	−24.34 ± 0.07	−6.0 ± 0.1
10	2	91.0 ± 0.5	0.521 ± 0.026	0.452	−20.60 ± 0.08	−31.20 ± 0.01	−8.1 ± 0.1
NaCl added							
NA-1	3	23.5 ± 0.5	0.689 ± 0.003	0.637*	−8.57 ± 0.16	−18.21 ± 0.06	−6.8 ± 0.2
NA-2	3	25.7 ± 0.5	0.698 ± 0.008	0.646*	−8.70 ± 0.16	−18.50 ± 0.07	−6.4 ± 0.2
NA-3	1	37.5 ± 0.5	0.639 ± 0.020	0.587*	−11.29 ± 0.20	−20.39 ± 0.10	−6.8 ± 0.1
NA-4	3	37.5 ± 0.5	0.672 ± 0.027	0.603	−13.30 ± 0.37	−26.06 ± 0.18	−8.8 ± 0.4
NA-5	2	49.6 ± 0.5	0.605 ± 0.005	0.553*	−13.85 ± 0.26	−21.39 ± 0.03	−7.2 ± 0.3
NA-6	3	49.6 ± 0.5	0.634 ± 0.008	0.565	−15.06 ± 0.22	−25.26 ± 0.17	−8.4 ± 0.2
NA-7	3	69.9 ± 0.5	0.577 ± 0.010	0.525*	−16.92 ± 0.15	−21.71 ± 0.03	−7.0 ± 0.2
NA-8	3	79.9 ± 0.5	0.553 ± 0.018	0.501*	−17.54 ± 0.03	−25.86 ± 0.10	−6.3 ± 0.1
NA-9	5	91.0 ± 0.5	0.545 ± 0.005	+	−19.21 ± 0.15	−25.00 ± 0.16	−6.3 ± 0.2

Table 5
Δ_{47}, $\delta^{18}O$, and $\delta^{13}C$ values of carbonates precipitated in the pressurized reaction vessel from a mixed solution of $CaCl_2$ and $NaHCO_3$. $\delta^{18}O_{water}$ is the back-calculated solution isotope value based on the carbonate $\delta^{18}O$ value and the fractionation factors corresponding to the mineralogy of the analysed samples and the experimental temperature. *n* indicates the number of replicate samples analysed. $\Delta_{47,uncorrected}$ gives the sample value without acid correction (all digested at 90 °C). Uncertainties for Δ_{47} measurements are given as standard error (1 SE) and as 1σ standard deviation for $\delta^{18}O$, $\delta^{13}C$ and $\delta^{18}O_{water}$.

Experiment No.	*n* (-)	T (°C)	Δ_{47} (‰)	$\Delta_{47,uncorrected}$ (‰)	$\delta^{18}O$ (‰)	$\delta^{13}C$ (‰)	$\delta^{18}O_{water}$ (‰)
Reaction vessel							
R-1	4	25 ± 2	0.702 ± 0.011	0.633	−6.72 ± 0.09	2.08 ± 0.05	−4.6 ± 0.1
R-2	5	50 ± 2	0.624 ± 0.008	0.555	−11.52 ± 0.19	1.86 ± 0.05	−4.7 ± 0.2
R-3	5	80 ± 2	0.572 ± 0.008	0.503	−15.60 ± 0.10	1.08 ± 0.04	−4.5 ± 0.1
R-4	5	100 ± 2	0.550 ± 0.010	0.481	−18.36 ± 0.23	−0.58 ± 0.09	−4.2 ± 0.2
R-5	5	125 ± 2	0.501 ± 0.013	0.432	−21.26 ± 0.13	−1.73 ± 0.25	−4.1 ± 0.1
R-6	5	150 ± 2	0.478 ± 0.008	0.409	−23.24 ± 0.26	−2.02 ± 0.09	−3.5 ± 0.3
R-7	5	175 ± 2	0.451 ± 0.010	0.382	−21.48 ± 0.12	−2.25 ± 0.06	0.7 ± 0.1
R-8	5	200 ± 2	0.430 ± 0.011	0.361	−21.21 ± 0.30	−2.75 ± 0.13	3.1 ± 0.3
R-9	5	225 ± 2	0.412 ± 0.004	0.343	−28.50 ± 0.26	−2.50 ± 0.07	−2.5 ± 0.3
R-10	5	250 ± 2	0.390 ± 0.014	0.321	−28.50 ± 0.05	−2.77 ± 0.04	−0.8 ± 0.1

prevent early mineral formation. The latter process caused lower $\delta^{13}C$ values (mean: −25.6‰). The $\delta^{13}C$ values are further modified by the duration of the CO_2 bubbling and the equilibration temperature.

Acid-fractionation corrected Δ_{47} values vary between 0.390 ± 0.014‰ and 0.706 ± 0.010‰ corresponding to the experimental temperature range of 23 °C to 250 °C (Tables 4 and 5). Addition of NaCl results in no statistical significant deviation from $CaCO_3$ minerals that precipitated from a NaCl-free solution (Kluge et al., 2013a). Therefore, Δ_{47} values of minerals precipitated in the water bath with and without NaCl at the same temperature are combined to a mean value.

Average Δ_{47} values of the water bath follow a Δ_{47}-T slope of $4.00 \pm 0.20 \cdot 10^4/T^2$ (T in K; $R^2 = 0.97$; Supplementary Fig. S1) in the investigated temperature range of 23–91 °C. $CaCO_3$ minerals precipitated in the pressurized reaction vessel at 25–250 °C yield a Δ_{47}-T slope of $3.98 \pm 0.07 \cdot 10^4/T^2$ (T in K; $R^2 = 0.99$; Supplementary Fig. S2). A linear regression of the combined data set results in a slope of $3.80 \pm 0.07 \cdot 10^4/T^2$ (T in K; $R^2 = 0.99$).

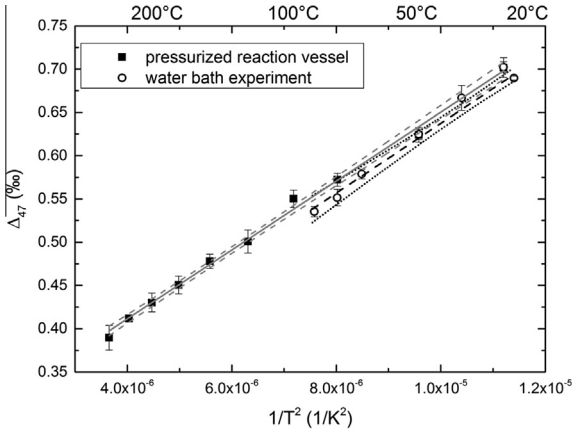

Fig. 2. Δ_{47}-temperature relationship of carbonates from the water bath and the pressurized reaction vessel. The sample values are displayed including a correction for the acid digestion reaction. Linear regressions are calculated separately for both data sets (solid line: pressurized reaction vessel, dashed line: water bath experiment). The confidence intervals for both experiments are given as dashed and short dotted lines, respectively.

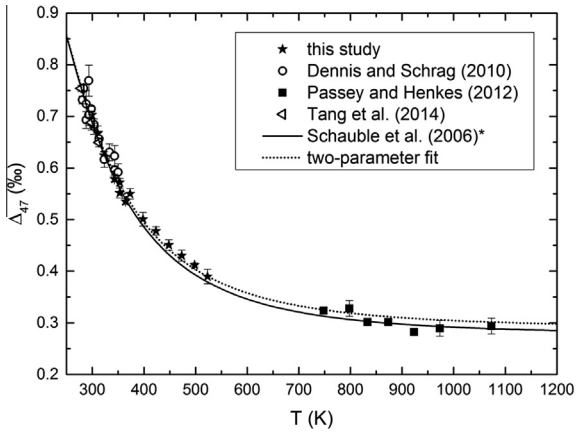

Fig. 3. Experimental Δ_{47}-T calibration data from inorganic laboratory precipitates of this study, Dennis and Schrag (2010), Passey and Henkes (2012), and Tang et al. (2014). These data are presented in the absolute reference frame of Dennis et al. (2011) and include a correction for the acid digestion as given in the respective publications. *The continuous line refers to the theoretical calculation for calcite of Schauble et al. (2006) using the acid-correction value of Passey and Henkes (2012). The two-parameter fit is also based on the Δ_{47}-T relationship of Schauble et al. (2006), but was fitted with regard to the constant term (i.e., acid fractionation) and includes a general scaling (see Eq. (3)).

5. DISCUSSION

5.1. Consistency between the two precipitation methods

Using two different methods for mineral precipitation enables the direct comparison of the results and provides constraints on the Δ_{47}-T relationship obtained from each experiment. Carbonates from the two different methods and temperature ranges (see Section 2) overlap in the temperature range between 20 and 80 °C. In order to compare both experimental approaches linear regression were calculated separately. The slopes of the linear regression of water bath and pressurized reaction vessel experiment (4.00 ($\pm$0.20)·$10^4/T^2$ and 3.98 ($\pm$0.07)·$10^4/T^2$, respectively; T in K) overlap at the 95% confidence level within their common experimental range (Fig. 2). Only the 80 °C and 90 °C sample in the water bath experiment show slightly lower Δ_{47} values compared to the regression line of data from the pressurized reaction vessel. All other water bath samples are close to or fall within the 95% confidence interval of the regression line of the data from the pressurized reaction vessel. The agreement of both approaches confirms the measured Δ_{47} values to be a primary temperature signal that is negligibly or not influenced by the specific mineral precipitation method.

5.2. High temperature Δ_{47} calibration

For theoretical considerations a 4th-order polynomial for the Δ_{47}-T curve was used (Schauble et al., 2006; Guo et al., 2009):

$$\Delta_{47} = -3.407 \cdot 10^9/T^4 + 2.365 \cdot 10^7/T^3 - 2.607 \cdot 10^3/T^2 - 5.880/T + 0.280 \quad (2)$$

The constant term in Eq. (2) refers to the shift in the Δ_{47} values due to the phosphoric acid digestion of carbonates (that produces CO_2 which is analyzed by mass spectrometry). Passey and Henkes (2012) experimentally determined the constant term in the reference frame of Dennis et al. (2011). The general relationship of Eq. (2) and its curvature with the constant term transferred into the absolute reference frame (0.280) follows closely our own data (Fig. 3). Furthermore, we combine our data with those of Dennis and Schrag (2010), Passey and Henkes (2012), and Tang et al. (2014) as all four studies used carbonates precipitated in the laboratory and applied high phosphoric acid reaction temperatures above 70 °C. This compilation provides a well-constrained, inter-laboratory Δ_{47}-T calibration for calcite over a large temperature range. All data follow a similar Δ_{47}-T relationship close to the theoretical curve and exhibit a similar curvature (Fig. 3). We therefore performed a two-parameter fit adjusting the theoretical curve (Eq. (2)) with regard to the constant term and a general scaling using an error-weighted least square regression. The best fit was obtained for scaling factor of 0.98 ($\pm$0.01) and constant term of 0.293 ($\pm$0.004) (Δ_{47} in ‰, T in K; $R^2 = 0.99$):

$$\Delta_{47} = 0.98 \cdot (-3.407 \cdot 10^9/T^4 + 2.365 \cdot 10^7/T^3 - 2.607 \cdot 10^3/T^2 - 5.880/T) + 0.293 \quad (3)$$

Only fitting the constant term in the theoretical curve to the experimental data (without any scaling) leads to an almost identical value of the constant term of 0.287 ($\pm$0.002). The individual experimental data points show a normal distribution relative to the regression line (Fig. S3). For comparison of theoretical values and experimental data note that the uncertainty in the theoretical calculations of Schauble et al. (2006) and Guo et al. (2009) is estimated to be on the order of 0.01‰.

This data shows that a unique Δ_{47}-T calibration exists for $CaCO_3$, independent of the method with which the minerals were precipitated (mixing of $CaCl_2$ and $NaHCO_3$ versus super-saturated $CaCO_3$ solution) or prepared (heating of carbonates at high temperatures for re-ordering experiments, Passey and Henkes, 2012). We therefore suggest Eq. (3) as reference Δ_{47}-T calibration for calcite that is acid digested at temperatures above 70 °C.

5.2.1. Linear approximation of the Δ_{47}-T relationship

An easier to use, linear form of the Δ_{47}-T relationship of this study combined with the results of Dennis and Schrag (2010), Passey and Henkes (2012) and Tang et al. (2014) can be derived in the $1/T^2$ space ($R^2 = 0.99$, Fig. 4):

$$\Delta_{47} = 3.97(\pm 0.03) \cdot 10^4/T^2 + 0.248(\pm 0.002) \quad \text{T in K, } \Delta_{47} \text{ in ‰} \tag{4}$$

An error-weighted linear regression over $1/T^2$ only based on the data of this study leads to an equation ($3.80\ (\pm 0.07)\cdot 10^4/T^2 + 0.259\ (\pm 0.006)$, $R^2 = 0.99$) that follows closely the linearized equation of the combined data set (Table 1), suggesting general agreement with the data of Passey and Henkes (2012), Dennis and Schrag (2010), and Tang et al. (2014).

Eq. (4) is given for comparison with published Δ_{47}-T relationships, but represents an approximation to the theoretical curvature of the Δ_{47}-T relationship and is therefore only valid within the experimental temperature range of this study. The linearized form (Eq. (4)) marginally deviates from the 4th order polynomial Eq. (3) in the experimental temperature range (≤0.005‰). Note that differences between the two curves can be significant outside this interval, e.g., ~0.01‰ at >600 °C, as the Δ_{47}-T slope gradually flattens at higher temperatures approaching a stochastic distribution (see e.g., Wang et al., 2004).

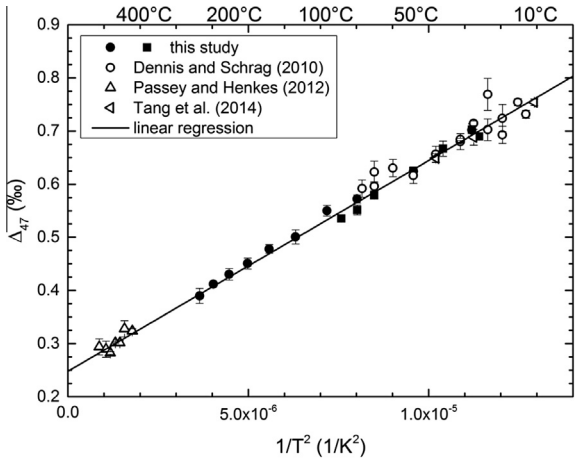

Fig. 4. Comparison of various empirical Δ_{47}-T calibrations that used a phosphoric acid digestion at high temperatures (≥70 °C). The values are given including the correction for the fractionation during phosphoric acid reaction. The linear regression follows Δ_{47} (T) = 0.397 (±0.003)·10⁵/T² + 0.248 (±0.002) ($R^2 = 0.996$, Δ_{47} in ‰, T in K).

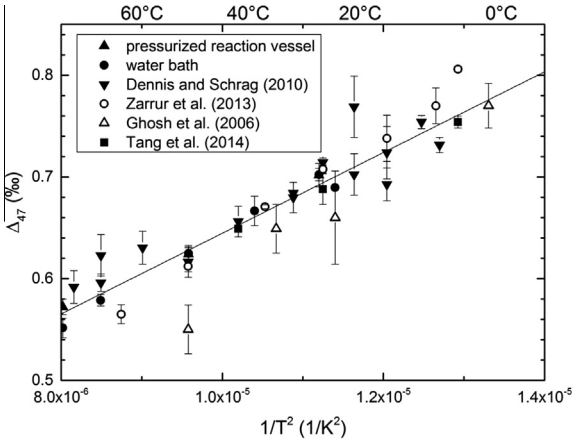

Fig. 5. Low-temperature range of experimental Δ_{47}-T calibrations. Despite significant scatter most data points are close to the linear regression of samples digested at high phosphoric acid temperature (≥70 °C, Eq. (4), black line).

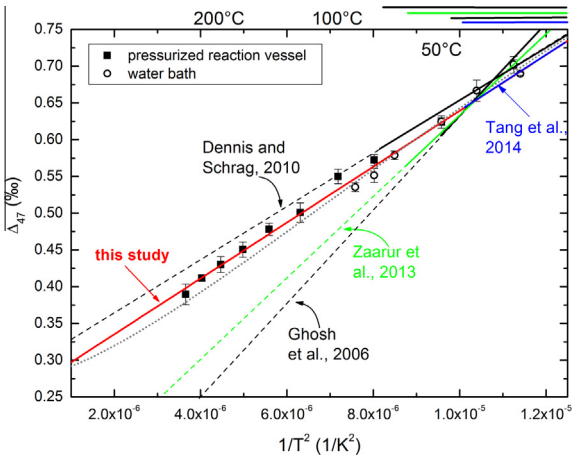

Fig. 6. Comparison of various experimental Δ_{47}-T calibrations. Our high-temperature data favor a relationship determined by theoretical models (e.g., Schauble et al., 2006; short dotted grey line). Solid lines on the top right corner indicate the calibration data range of the experimental studies. The dashed lines illustrate the extrapolation of the Δ_{47}-T relationships beyond their calibration ranges (see also Table 1). The linear regression of our study is close to model predictions of Schauble et al. (2006; acid fractionation factor after Passey and Henkes, 2012).

5.2.2. Comparison with published Δ_{47}-T relationships

In order to compare the Δ_{47} results of the laboratory precipitates of this study with literature data, it was necessary to correct for the difference in acid fractionation between 25 °C (original calibration of Ghosh et al., 2006) and 90 °C (see Section 3.3, Tables 4 and 5). After normalizing all data to the 25 °C acid reaction individual data points below 100 °C are hardly distinguishable from the calibration of Ghosh et al. (2006) and Zaarur et al. (2013) (Fig. 5). Whereas the individual data points of Ghosh et al. (2006) seem to deviate significantly at the upper end of Earth surface temperatures (50 °C), the recent calibration data of Zaarur et al. (2013) are close to the regression

line of this study. Despite the proximity of the individual data points to the temperature relationship defined in this study, the regression of the Zaarur et al. (2013) and Ghosh et al. (2006) data result in statistically different slopes for mineral formation in the low-temperature range of 5–80 °C (Figs. 5 and 6; Table 1). In contrast, the Δ_{47}-T relationship of Dennis and Schrag (2010) agrees well with data acquired in pressurized reaction vessel and water bath, which is visible in the similarity of the regression slopes.

Note that the calibrations of Ghosh et al. (2006), Dennis and Schrag (2010), and Zaarur et al. (2013) were obtained for a temperature range of 1–50 °C or ~77 °C, respectively, and therefore lead to large uncertainties and potentially wrong values if extrapolated to higher temperatures. The range of Δ_{47} values at 250 °C that would be within the uncertainty of the extrapolated Δ_{47}-T lines is 0.167 to 0.307‰, 0.399 to 0.450‰, and 0.241 to 0.321‰ in these three studies, respectively (Fig. 6). Our data defines the actual Δ_{47} values up to 250 °C and significantly reduces the uncertainty in this range from about 0.05–0.14‰, using the inadequate extrapolation of existing low-temperature studies, to <0.01‰ based on the 95% confidence interval of the linear regression of our data.

The Δ_{47}-T slope versus $1/T^2$ is about 3.80 ($\pm$0.07)·10^4 using only the results of this study, and 3.97 ($\pm$0.03)·10^4 including the data of Dennis and Schrag (2010), Passey and Henkes (2012), and Tang et al. (2014). These slopes are significantly lower than that of Ghosh et al. (2006; $6.39 \pm 0.49 \cdot 10^4$) or Zaarur et al. (2013; $5.55 \pm 0.27 \cdot 10^4$). The slope agrees well with the theoretical value of $4.05 \cdot 10^4$, that was fitted linearly to the predictions of Guo et al. (2009) from 0 to 250 °C (Table 1).

Deviations between the calibration of this study (Eqs. (3) and (4); Table 1) and the values of Ghosh et al. (2006) and Zaarur et al. (2013) may be related to differences in the details of the acid digestion procedure. In contrast to our setup, where samples are generally digested at 90 °C and the evolving CO_2 continuously collected, Ghosh et al. (2006) and Zaarur et al. (2013) reacted carbonates at 25 °C overnight and in a closed reaction vessel. Results of Dennis and Schrag (2010) and Passey and Henkes (2012), that used the same or a similar way of acid digestion and CO_2 gas processing as in our study, agree within uncertainty (Figs. 3 and 4).

5.3. High-temperature calibration curve for 90°C acidification temperature

Eq. (3) took into consideration the difference between an acid reaction at 25 °C and 90 °C, which is the traditional way that clumped isotope data are presented. Given the fact that most clumped isotope laboratories now use a 90 °C acid reaction temperature, here we give the Δ_{47}-T calibration line without acid fractionation. For each laboratory calibration using high-temperature (90 °C) on-line acid digestion methods (this study; Dennis and Schrag, 2010; Passey and Henkes, 2012) we subtracted the acid fractionation correction that was specifically applied in these labs for normalization to a 25 °C acid reaction. Therefore, for all experiments that digest carbonates at 90 °C using the on-line method and continuous collection of CO_2 this specific calibration line can directly be used for temperature determination without further adjustment by an acid-fractionation correction (Fig. S4):

$$\Delta_{47} = 4.05(\pm 0.04) \cdot 10^4/T^2 + 0.167(\pm 0.002) \quad T \text{ in K}, \Delta_{47} \text{ in ‰} \tag{5}$$

In case of our study we only included samples for which all replicates were reacted at 90 °C (Tables 4 and 5).

The difference between the intercepts of Eqs. (4) and (5) and with the intercept of theoretical models (Schauble et al., 2006; Guo et al., 2009) is due to the correction applied for the acid fractionation. The theoretical value of the acid fractionation correction of 0.069‰ at 90 °C (Guo et al., 2009) deviates from empirically determined values of e.g., 0.092‰ in the study of Henkes et al. (2013), 0.081‰ in the studies of Passey and Henkes (2012), but is close to the results of Wacker et al. (2013) of 0.070‰. The acid fractionation correction for clumped isotopes relative to a 25 °C phosphoric acid reaction cannot be consistently assessed by comparing the 90 °C acid digestion results of this study with the calibration data of Ghosh et al. (2006) and Zaarur et al. (2013), that are based on a 25 °C acid digestion, as the calibration curves intersect (Supplementary Fig. S5). We therefore evaluate the acid fractionation correction by comparison with the theoretical model of Guo et al. (2009) that yields a similar curvature. Adding an acid fractionation correction of 0.07–0.09‰ to the initially acid-correction-free Eq. (4) provides a reasonable match between the empirical results and the theoretical prediction of Guo et al. (2009). The range of appropriate values for the acid fractionation overlaps with the theoretical prediction (0.069‰; Guo et al., 2009). For a more precise future determination of the acid fractionation relative to 25 °C reactions (i.e., the temperature dependence of the acid fractionation), carbonates that grew over a large temperature range and that exhibit a large range in $\delta^{18}O$ and $\delta^{13}C$ values need to be analyzed at acid digestion temperatures of both 25 and 90 °C.

5.4. Evaluation of potential isotopic effects during carbonate precipitation

Using the laboratory carbonate data to establish a precise Δ_{47}-T calibration all samples potentially affected by non-equilibrium isotopic effects during mineral formation need to be excluded. Disequilibrium effects could mask the true Δ_{47}-T relationship. Non-equilibrium effects could be related to early mineral formation when the solution has not yet reached isotopic equilibrium. Furthermore, rapid mineral formation can induce isotopic disequilibrium due to preferential incorporation of light isotopes (Watson, 2004; Dietzel et al., 2009; Watson and Müller, 2009; DePaolo, 2011; Reynard et al., 2011; Gabitov et al., 2012; Gabitov, 2013). Increased concentrations of certain ions cause an isotopic differentiation between water molecules 'bound' to ions and 'free' bulk water (Taube, 1954; Sofer and Gat, 1972; O'Neil and Truesdell, 1991), however, this was found not to affect carbonate clumped isotopes for Na^+, Cl^-, Mg^{2+} and low concentrations of Ca^{2+} (Kluge

et al., 2013a). The solution inside the pressurized reaction vessel has a low Ca^{2+} concentration of $\leqslant$0.1 mol/l and is therefore expected not to affect the clumped isotope value. Fast CO_2 degassing from a CO_2-rich solution can cause significant disequilibrium effects of up to several ‰ in $\delta^{18}O$ and up to 0.08‰ in Δ_{47} (Guo, 2008; Daëron et al., 2011; Kluge and Affek, 2012; Kluge et al., 2013b). In addition, mineral formation during fast physico-chemical changes (e.g. during de-pressurization of the reaction vessel) could lead to a disequilibrium signal. For example, de-pressurization could lead to partial evaporation and degassing of the solution and to strong kinetic isotope fractionation that may be recorded during related mineral formation. Furthermore, re-ordering of isotopes in the mineral at temperatures above the closure temperature for clumped isotopes (estimated at above 100 °C) could impact on the apparent Δ_{47} value of the experiment (Dennis and Schrag, 2010; Passey and Henkes, 2012; Henkes et al., 2014), in particular, during the time period at which the precipitated crystals were cooled down from high experiment temperatures (200–250 °C) for sampling.

5.4.1. Rapid mineral formation

Rapid mineral precipitation as a potential cause for variable and measurable disequilibrium in Δ_{47} has to be investigated for the two applied precipitation techniques. Observations of the experiment progress in the water bath experiment (precipitation from a super-saturated $CaCO_3$ solution by slow N_2 bubbling; Kluge et al., 2013a; Supplementary Material) showed that the first minerals typically precipitate after ~0.5 day. The minimum experiment duration was 20 h, but lasted typically 130 h and resulted in about ~140 mg (1400 μmol) of carbonate. Considering a surface area of the beaker of 0.02 m^2 it corresponds to an average precipitation rate of 490 μmol m^{-2} h^{-1}. Comparable growth rates were observed in similar laboratory experiments (Dietzel et al., 2009; Gabitov et al., 2012; Watkins et al., 2013). Although these growth rates can induce strong isotopic disequilibrium with regard to $\delta^{18}O$ (Dietzel et al., 2009; Gabitov et al., 2012; Gabitov, 2013; Watkins et al., 2013), no such effect has been observed for Δ_{47} in the case of moderate growth rates of up to several 100 μmol m^{-2} h^{-1} in speleothems (Kluge and Affek, 2012) and inorganic carbonates from laboratory experiments (Tang et al., 2014; using the same samples as Dietzel et al., 2009).

The precipitation rate was controlled in the water bath experiment by slow N_2 bubbling (~1 bubble per s) and, in general, prevented rapid mineral precipitation. In similar experiments Kim and O'Neil (1997) and Ghosh et al. (2006) used bubbling rates of 0.3–0.8 bubbles per second. Minerals in the pressurized reaction vessel formed in a closed atmosphere similarly preventing uncontrolled rapid changes in the solution composition and kept the growth rate in a limited range. First order estimates of the growth rate lead to values of 2100 μmol m^{-2} h^{-1} based on a surface area of 0.01 m^2 and an average precipitated amount of 250 mg during 120 h experiment duration. Note that this value is only an average estimate as the growth rate was likely higher at the time of solution injection and decreased afterwards. In essence, the mineral growth rate in the pressurized reaction vessel is higher than the growth rate estimate from the water bath experiment, overlapping with rates at which effects were first observed for corals. Saenger et al. (2012) noticed significant Δ_{47} offsets of up to +0.05‰ in hermatypic corals that grew rapidly (>1000 μmol m^{-2} h^{-1}). Thus, we cannot *a priori* exclude an effect for the pressurized reaction vessel. However, by comparing the Δ_{47} results from the pressurized reaction vessel and water bath in their common interval from 25 °C to 80 °C, where they are either identical or overlapping within measurement uncertainties (Fig. 2), at most a limited effect of the higher growth rate in the pressurized reaction vessel can be deduced (on the order of 0.01‰). This is consistent with measurements of Tang et al. (2013) that investigated the same samples used by Dietzel et al. (2009) to study the growth rate effect on $\delta^{18}O$. In contrast to the significant effects in $\delta^{18}O$, no offsets were found for Δ_{47} (Tang et al., 2013, 2014).

5.4.2. Fast CO_2 degassing

Disequilibrium effects due to degassing as observed for speleothems (e.g. Daëron et al., 2011; Kluge and Affek, 2012) can be ruled out due to several reasons. Carbonates grow on the top of stalagmites from a thin water film on the order of 100 μm (Dreybrodt, 1980) which leads to fast degassing of the CO_2-supersaturated drip water (within few seconds; e.g., Dreybrodt and Scholz, 2011) and which causes an initial isotopic disequilibrium. In contrast, the water depth is significantly greater for the laboratory experiments considered here (~10 cm in the water bath; 5 cm in the pressurized reaction vessel). The atmosphere above the Erlenmeyer flask in the water bath experiment is well controlled. Gas flux from the solution through the small gas space (100 ml) to the atmosphere is only possible through a thin tube (radius ~2 mm) and is controlled via slow N_2 bubbling. The controlled slow gas flow is not expected to cause rapid changes in the solution CO_2 concentration. The large ratio of water (~500 ml) relative to the gas flux (1 bubble/s corresponding to $\leqslant$0.03 ml) suggests a negligible effect on the isotopic values of the DIC. Mineral formation in the pressurized reaction vessel proceeded in a closed system without active gas flow. The atmosphere in the reaction vessel was pressurized with N_2 tank gas, but changed according to the chemical changes in the added solution. CO_2 escapes from the mixed and stirred solution until equilibrium between the gas space and the solution in the pressurized reaction vessel is reached. Due to the relatively large solution volume (100 ml) compared to the gas space directly above the solution of ~200 ml significant and persistent degassing in unlikely. An initial isotopic disequilibrium due to gas exchange between solution and N_2 atmosphere in the pressurized reaction vessel quickly reaches equilibrium values in the DIC due to the short time scales for isotopic equilibration at high temperatures. Equilibrium between oxygen isotopes in water and DIC takes about 9 h at 25 °C and pH 8–8.7, whereas it is less than 2 h at temperatures above 40 °C (Beck et al., 2005). Extrapolating the data of Beck to 100 °C suggests oxygen isotope equilibrium to be reached in less than 1 min, and within seconds at 250 °C.

5.4.3. Disequilibrium during depressurization

The precipitation experiments at temperatures above 80 °C were performed under high pressures of up to 80 bar in a closed system. The collection of minerals requires depressurization and cooling-down of the system. It could lead to disequilibrium carbonate precipitation due to rapid physico-chemical changes during depressurization. Reduced pressure combined with still high temperatures can lead to the evaporation of the liquid, degassing and to an increase in the $CaCO_3$ concentration inducing carbonate precipitation. We attempted to prevent this effect using two different approaches.

First, we used the internal pressure of the system (provided by a N_2 gas tank) to push the solution out of the pressurized reaction vessel through the injection tubing by opening a valve at fluid pump A (see Fig. 1A). A fine filter (pore size: 0.5 μm; Upchurch Scientific) prevented the calcite crystals from being flushed out. Closing the N_2 gas tank slowly decreased the pressure. Before the pressure reached the boiling point, the complete solution or most of the solution had already left the pressurized reaction vessel. Based on the short times scales of fluid extraction (few minutes) and the still high pressure in the vessel after the fluid left through the capillaries, negligible carbonate precipitation related to these disequilibrium conditions is expected during depressurization. The second approach was applied after long precipitation periods that ensured that the majority of minerals were already formed and that the $CaCO_3$ super-saturation reached low levels. The system was cooled down to values between 20 and 60 °C before depressurization of the system. This avoids boiling of the solution during depressurization and together with already low levels of super-saturation does not provide additional carbonate minerals to the existing assemblage during the cool-down. This method was applied in the experiments R5, R6, R7, R8, R10 (Table 3) and ensured the contribution of minerals related to the depressurization and cooling-down to be minimal.

5.4.4. Isotope re-ordering effects

At experimental temperatures above 100 °C the effect of isotope re-ordering has to be assessed. The closure temperature for calcite, below which isotope re-ordering is irrelevant, was found to be 100–150 °C (Dennis and Schrag, 2010; Schmid and Bernasconi, 2010; Passey and Henkes, 2012; Henkes et al., 2014). Isotope exchange between the different $CaCO_3$ isotopologues at temperatures above 100 °C can lead to variations in the Δ_{47} value, notably higher Δ_{47} values, corresponding to lower temperatures during the cooling process (before the precipitated crystals are filtered and dried). The cooling process of the pressurized reaction vessel before sample filtration took about 1 h.

The rate constant of the isotope exchange reaction during solid state reordering decreases rapidly with decreasing temperatures, e.g., five orders of magnitude from 250 °C to 150 °C (using experimental data for optical calcite of Passey and Henkes, 2012). Estimating the re-ordering effect during the 1 h cooling-down process from 250 °C to 150 °C leads to a negligible change of $<10^{-8}$ ‰ (for details see Supplementary Material). Only a much lower cooling rate (for example, 1 K per 100 a) and a longer overall cooling period (for example 1500 a) would cause a small, but still hardly measureable effect (~0.002‰ for this cooling rate and a time period of 1500 a). We can thus safely neglect any influence of reordering effects during the time period of sample cool down.

5.4.5. Calculated solution oxygen isotope values as a control on isotopic effects

For all experiments highly pure water based on reverse osmosis with an 18 MΩ cm resistance was used. It is directly sourced from the local tap water before being purified. Therefore, we used the regional groundwater and surface water $\delta^{18}O$ value of −6‰ to −7‰ (Darling et al., 2003) as reference for the solution $\delta^{18}O$ value (note, the solution $\delta^{18}O$ value was not analyzed in this study). The solution $\delta^{18}O$ value of the two experimental setups was back-calculated from the measured carbonate $\delta^{18}O$ values and the experimental temperatures using the fractionation factors corresponding to the $CaCO_3$ mineral (see Section 3.3). The mean of the water bath experiment of -6.9 ± 0.9‰ (Table 4) agrees well with the groundwater/surface water value of Darling et al. (2003). Together with the absence of $\delta^{18}O$ trends with temperature (Fig. S6), precipitation or equilibration time this suggests no unrecognized disequilibrium fractionation to have occurred during this set of experiments.

In contrast, the solution $\delta^{18}O$ value in the pressurized reaction vessel is more positive and shows a trend toward increasingly positive values at higher temperatures (Table 5). This effect can be explained by evaporation and a re-distribution of water molecules between the solution and an initially pure and water-free N_2 gas phase above the solution. Theoretically, this process progresses until saturation with water vapor is reached. Higher experiment temperatures cause a higher partial pressure of water vapor and enable a higher absolute amount of water to be contained in the gas phase before saturation is reached. For instance, air at 20 °C is saturated at 15 g H_2O/kg air, whereas it can hold up to 280 g H_2O/kg air at 70 °C and 1 bar (Baehr, 1988). The oxygen isotopes in the solution change due to the transition of water from the solution into the gas phase. The light isotopes are the kinetically faster component, which eventually leads to an enrichment of ^{18}O in the remaining solution. A comparison of the back-calculated solution $\delta^{18}O$ value with the amount of evaporated water gives a good correlation and supports this explanation (Fig. S7, Supplementary Material).

The change in the apparent $\delta^{18}O$ value of the solution does not necessarily indicate mineral formation in isotopic disequilibrium. The saturation of the N_2 gas atmosphere in the pressurized reaction vessel happens quickly after the injection of the diluted $NaHCO_3$ and $CaCl_2$ solutions starts. The diffusion coefficient of water vapor in air is $\sim 2.8 \cdot 10^{-5}$ m^2/s at 25 °C (Cussler, 1997) and thus reaches a diffusion length of 5 cm, corresponding to the dimensions of the gas space in the pressurized reaction vessel, in less than 1 min. In addition, at low temperatures of 25, 50 and 80 °C only a small relative water fraction redistributes into the gas space (0.003, 0.01, and 0.08 ml, respectively,

relative to 100 ml solution). This fraction is larger at higher temperatures, but the oxygen isotope exchange between water and the DIC is fast at experiment temperatures above 100 °C. The oxygen isotope exchange reaction between water and DIC has a time constant of 9 h at 25 °C (Beck et al., 2005) and decreases rapidly at higher temperatures, e.g., to few minutes at 100 °C. The fast re-equilibration of the oxygen isotopes between DIC and water in the mixed solution, after the water-saturation of the gas phase is completed, suggests that the clumped isotope values are unaffected by secondary effects and primarily reflect the mineral formation temperature.

6. CONCLUSIONS

The good agreement of laboratory Δ_{47}-T calibration data of this study with Δ_{47} values acquired in other experiments by digesting synthetic carbonates at 90 °C indicates that a common Δ_{47}-T calibration exists for inorganic carbonates, if evaluated in the absolute reference frame and using the same acid digestion temperature with active CO_2 removal. The slope of the experimental data agrees well with predicted theoretical values.

This new and extended empirical Δ_{47}-T calibration curve provides a solid basis for the application of the carbonate clumped isotope proxy to the temperature range from 20 to 250 °C (from 7.5 to 800 °C, including the data of Dennis and Schrag (2010), Passey and Henkes (2012) and Tang et al. (2014)) and, thus, to relevant questions related to high-temperature geological processes.

ACKNOWLEDGEMENTS

We gratefully acknowledge funding from the Qatar Carbonates and Carbon Storage Research Centre (QCCSRC), provided jointly by Qatar Petroleum, Shell, and Qatar Science and Technology Park. T. Kluge was additionally supported by the Heidelberg Graduate School of Fundamental Physics. We thank the Carbonate Research group at Imperial College for fruitful discussions, Matt Andrews and Gavin Barnes for technical assistance in assembling and initializing the high-temperature setup, and Jens Najorka for assistance and advice during XRD measurements at the National History Museum London. We thank three anonymous reviewers and the associate editor E. Schauble for their constructive comments that helped to improve the manuscript.

APPENDIX A. SUPPLEMENTARY DATA

Supplementary data associated with this article can be found, in the online version, at http://dx.doi.org/10.1016/j.gca.2015.02.028.

REFERENCES

Affek H. P. (2012) Clumped isotope paleothermometry: principles, applications and challenges. In: *Reconstructing Earth's deep-time climate – the state of the art in 2012*. (eds. L. C. Ivany and B. T. Huber). The Paleontological Society Papers, Vol. 18, pp. 101–114.

Affek H. P. and Eiler J. M. (2006) Abundance of mass 47 CO_2 in urban air, car exhaust and human breath. *Geochim. Cosmochim. Acta* **70**, 1–12.

Baehr H. D. (1988) *Thermodynamik*. Springer Verlag, Berlin, Heidelberg.

Beck W. C., Grossman E. L. and Morse J. W. (2005) Experimental studies of oxygen isotope fractionation in the carbonic acid system at 15, 25 and 40 °C. *Geochim. Cosmochim. Acta* **69**, 3493–3503.

Bergman S., Huntington K. and Winterleitner G. (2010) Carbonate clumped isotope thermometry as a tool to constrain thermal conditions in the shallow crust during deformation and diagenesis, Paradox Basin, Utah. *GSA Annual Meeting Abstract* **42**, 473.

Böhm F., Joachimski M. M., Dullo W. C., Eisenhauer A., Lehnert H., Reitner J. and Worheide G. (2000) Oxygen isotope fractionation in marine aragonite of coralline sponges. *Geochim. Cosmochim. Acta* **64**, 1695–1703.

Bristow T. F., Bonifacie M., Derkowski A., Eiler J. M. and Grotzinger J. P. (2011) A hydrothermal origin for isotopically anomalous cap dolostone cements from south China. *Nature* **474**, 68–72.

Budd D. A., Frost, III, E. L., Huntington K. W. and Allwardt P. F. (2013) Syndepositional deformation features in high-relief carbonate platforms: long-lived conduits for diagenetic fluids. *J. Sed. Res.* **82**, 12–36.

Cao X. and Liu Y. (2012) Theoretical estimation of the equilibrium distribution of clumped isotopes in nature. *Geochim. Cosmochim. Acta* **77**, 292–303.

Cussler E. L. (1997) Diffusion – mass transport in fluid systems. Cambridge Univ. Press, second edition, New York.

Daëron M., Guo W., Eiler J. M., Genty K., Blamart D., Boch R., Drysdale R. N., Maire R., Wainer K. and Zanchetta G. (2011) 13C–18O clumping in speleothems: Observations from natural caves and precipitation experiments. *Geochim. Cosmochim. Acta* **75**, 3303–3317.

Dale A., John C. M., Mozley P., Smalley P. C. and Muggeridge A. H. (2014) Time-capsule concretions: unlocking burial diagenetic processes in the Mancos Shale using carbonate clumped isotopes. *Earth Planet. Sci. Lett.* **394**, 30–37.

Darling W. G., Bath A. H. and Talbot J. C. (2003) The O&H stable isotopic composition of fresh waters in the British Isles. 2. Surface waters and groundwater. *Hydrol. Earth Sys. Sci.* **7**, 183–195.

Dennis K. J. and Schrag D. P. (2010) Clumped isotope thermometry of carbonatites as an indicator of diagenetic alteration. *Geochim. Cosmochim. Acta* **74**, 4110–4122.

Dennis K. J., Affek H. P., Passey B. H., Schrag D. P. and Eiler J. W. (2011) Defining an absolute reference frame for 'clumped' isotope studies of CO_2. *Geochim. Cosmochim. Acta* **75**, 7117–7131.

DePaolo D. J. (2011) Surface kinetic model for isotopic and trace element fractionation during precipitation of calcite from aqueous solutions. *Geochim. Cosmochim. Acta* **75**, 1039–1056.

Dreybrodt W. (1980) Deposition of calcite from thin films of natural calcareous solutions and the growth of speleothems. *Chem. Geol.* **29**, 89–105.

Dreybrodt W. and Scholz D. (2011) Climatic dependence of stable carbon and oxygen isotope signals recorded in speleothems: from soil water to speleothem calcite. *Geochim. Cosmochim. Acta* **75**, 734–752.

Dietzel M., Tang J., Leis A. and Köhler S. J. (2009) Oxygen isotopic fractionation during inorganic calcite precipitation – effects of temperature, precipitation rate and pH. *Chem. Geol.* **268**, 107–115.

Eagle R. A., Eiler J. M., Tripati A. K., Ries J. B., Freitas P. S., Hiebenthal C., Wanamaker, Jr., A. D., Taviani M., Elliot M., Marenssi S., Nakamura K., Ramirez P. and Roy K. (2013) The influence of temperature and seawater carbonate saturation

state on 13C–18O bond ordering in bivalve mollusks. *Biogeosciences* **10**, 4591–4606.

Eiler J. M. (2007) "Clumped-isotope" geochemistry – the study of naturally-occurring, multiply-substituted isotopologues. *Earth Planet. Sci. Lett.* **262**, 309–327.

Eiler J. M. (2011) Paleoclimate reconstruction using carbonate clumped isotope thermometry. *Quat. Sci. Rev.* **30**, 3575–3588.

Eiler J. M. (2013) The isotopic anatomies of molecules and minerals. *Annu. Rev. Earth Planet. Sci.* **41**, 411–441.

Eiler J. M. and Schauble E. (2004) $^{18}O^{13}C^{16}O$ in Earth's atmosphere. *Geochim. Cosmochim. Acta* **68**, 4767–4777.

Ferry J. M., Passey B. M., Vasconcelos C. and Eiler J. M. (2011) Formation of dolomite at 40–80°C in the Latemar carbonate buildup, Dolomites, Italy, from clumped isotope thermometry. *Geology* **39**, 571–574.

Gabitov R. I. (2013) Growth-rate induced disequilibrium of oxygen isotopes in aragonite: an in situ study. *Chem. Geol.* **351**, 268–275.

Gabitov R. I., Watson E. B. and Sadekov A. (2012) Oxygen isotope fractionation between calcite and fluid as a function of growth rate and temperature: an in-situ study. *Chem. Geol.* **306–307**, 92–102.

Ghosh P., Adkins J., Affek H. P., Balta B., Guo W., Schauble E. A., Schrag D. and Eiler J. M. (2006) ^{13}C–^{18}O bonds in carbonate minerals: a new kind of paleothermometer. *Geochim. Cosmochim. Acta* **70**, 1439–1456.

Grauel A.-L., Schmid T. W., Hu B., Bergami C., Capotondi L., Zhou L. and Bernasconi S. M. (2013) Calibration and application of the 'clumped isotope' thermometer to foraminifera for high-resolution climate reconstructions. *Geochim. Cosmochim. Acta* **108**, 125–140.

Guo W. (2008) Carbonate clumped isotope thermometry: application to carbonaceous chondrites and effects of kinetic isotope fractionation. Ph. D. thesis, Caltech, USA.

Guo W., Mosenfelder J. L., Goddard, III, W. A. and Eiler J. M. (2009) Isotopic fractionations associated with phosphoric acid digestion of carbonate minerals: insights from first-principles theoretical modeling and clumped isotope measurements. *Geochim. Cosmochim. Acta* **73**, 7203–7225.

Henkes G. A., Passey B. H., Wanamaker, Jr., A. D., Grossman E. L., Ambrose, Jr., W. G. and Carrol M. L. (2013) Carbonate clumped isotope compositions of modern marine mollusk and brachiopod shells. *Geochim. Cosmochim. Acta* **106**, 307–325.

Henkes G. A., Passey B. H., Grossman E. L., Shenton B. J., Pérez-Huerta A. and Yancey T. E. (2014) Temperature limits for preservation of primary calcite clumped isotope paleotemperatures. *Geochim. Cosmochim. Acta* **139**, 362–382.

Huntington K. W., Eiler J. M., Affek H. P., Guo W., Bonifacie M., Yeung L. Y., Thiagarajan N., Passey B., Tripati A., Daëron M. and Came R. (2009) Methods and limitations of 'clumped' CO_2 isotope (Δ_{47}) analysis by gas-source isotope ratio mass spectrometry. *J. Mass Spectrom.* **44**, 1318–1329.

Huntington K. W., Budd D. A., Wernicke B. P. and Eiler J. M. (2011) Clumped-isotope thermometry to constrain the crystallization temperature of diagenetic calcite. *J. Sed. Res.* **81**, 656–669.

Kim S. T. and O'Neil J. R. (1997) Equilibrium and nonequilibrium oxygen isotope effects in synthetic carbonates. *Geochim. Cosmochim. Acta* **61**, 3461–3475.

Kim S.-T., O'Neil J. R., Hillaire-Marcel C. and Mucci A. (2007) Oxygen isotope fractionation between synthetic aragonite and water: influence of temperature and Mg^{2+} concentration. *Geochim. Cosmochim. Acta* **71**, 4704–4715.

Kluge T. and Affek H. P. (2012) Quantifying kinetic fractionation in Bunker Cave speleothems using Δ_{47}. *Quat. Sci. Rev.* **49**, 82–94.

Kluge T., John C. M. and Davis S. (2013a) Constraints for the clumped isotope application in diagenetic environments involving high salt concentrations. *Mineralog. Mag.* **77**(5), 1142.

Kluge T., Affek H. P., Marx T., Aeschbach-Hertig W., Riechelmann D. F. C., Scholz D., Riechelmann S., Immenhauser A., Richter D. K., Fohlmeister J., Wackerbarth A., Mangini A. and Spötl C. (2013b) Reconstruction of drip-water $\delta^{18}O$ based on calcite oxygen and clumped isotopes of speleothems from Bunker Cave (Germany). *Clim. Past* **9**, 377–391.

Loyd S. J., Corsetti F. A., Eiler J. M. and Tripati A. K. (2012) Determining the diagenetic conditions of concretion formation: assessing temperatures and pore waters using clumped isotopes. *J. Sed. Res.* **82**, 1006–1016.

McCrea J. M. (1950) On the isotopic chemistry of carbonates and a paleotemperature scale. *J. Chem. Phys.* **18**, 849–857.

O'Neil J. R. and Truesdell A. H. (1991) Oxygen isotope fractionation studies of solute-water interaction. In: *Stable isotope geochemistry: a tribute to Samuel Epstein* (eds. H. P. Taylor, J. R. O'Neil and I. R. Kaplan). The Geochemical Society, Special Publication No. 3, San Antonio, USA.

O'Neil J. R., Clayton R. N. and Mayeda T. K. (1969) Oxygen isotope fractionation in divalent metal carbonates. *J. Chem. Phys.* **51**, 5547–5558.

Passey B. H. and Henkes G. A. (2012) Carbonate clumped isotope bond reordering and geospeedometry. *Earth Planet. Sci. Lett.* **351–352**, 223–236.

Price J. B. and Eiler J. M. (2013) Crystallization temperatures of carbonate phases at Kennecott, Alaska based on clumped isotope thermometry. *Mineral. Mag.* **77**, 1997.

Reynard L. M., Day C. C. and Henderson G. M. (2011) Large fractionation of calcium isotopes during cave-analogue calcium carbonate growth. *Geochim. Cosmochim. Acta* **75**, 3726–3740.

Saenger C., Affek H. P., Felis T., Thiagarajan N., Lough J. M. and Holcomb M. (2012) Carbonate clumped isotope variability in shallow water corals: temperature dependence and growth-related vital effects. *Geochim. Cosmochim. Acta* **99**, 224–242.

Schauble E. A., Ghosh P. and Eiler J. M. (2006) Preferential formation of 13C–18O bonds in carbonate minerals, estimated using first-principle lattice dynamics. *Geochim. Cosmochim. Acta* **70**, 2510–2529.

Schmid T. W. and Bernasconi S. M. (2010) An automated method for 'clumped-isotope' measurements on small carbonate samples. *Rapid Commun. Mass Spectrom.* **24**, 1955–1963.

Sofer Z. and Gat J. R. (1972) Activities and concentrations of oxygen-18 in concentrated aqueous salt solutions: analytical and geophysical implications. *Earth Planet. Sci. Lett.* **15**, 232–238.

Swanson E. M., Wernicke B. P., Eiler J. M. and Losh S. (2012) Temperatures and fluids on faults based on carbonate clumped-isotope thermometry. *Am. J. Sci.* **312**, 1–21.

Tang J., Rosenheim B. E., Dietzel M., Fernandez A. and Tripati A. K. (2013) Evaluation of kinetic effect on clumped isotope fractionation (Δ_{47}) during inorganic calcite precipitation. *Mineral. Mag.* **77**, 2308.

Tang J., Dietzel M., Fernandez A., Tripati A. K. and Rosenheim B. E. (2014) Evaluation of kinetic effect on clumped isotope fractionation (Δ_{47}) during inorganic calcite precipitation. *Geochim. Cosmochim. Acta* **134**, 120–136.

Tarutani T., Clayton R. N. and Mayeda T. K. (1969) The effect of polymorphism and magnesium substitution on oxygen isotope fractionation between calcium carbonate and water. *Geochim. Cosmochim. Acta* **33**, 987–996.

Taube H. (1954) Use of oxygen isotope effects in the study of hydration of ions. *J. Chem. Phys.* **58**, 523–528.

Tripati A. K., Eagle R. A., Thiagarajan N., Gagnon A. C., Bauch H., Halloran P. R. and Eiler J. M. (2010) 13C–18O isotope signatures and 'clumped isotope' thermometry in foraminfera and coccoliths. *Geochim. Cosmochim. Acta* **74**, 5697–5717.

Uchikawa J. and Zeebe R. E. (2012) The effect of carbonic anhydrase on the kinetics and equilibrium of the oxygen isotope exchange in the CO_2–H_2O system: implications on the $\delta^{18}O$ vital effects in biogenic carbonates. *Geochim. Cosmochim. Acta* **95**, 15–34.

Wacker U., Fiebig J. and Schoene B. R. (2013) Clumped isotope analysis of carbonates: comparison of two different acid digestion techniques. *Rapid Commun. Mass Spectrom.* **27**, 1631–1642.

Wang Z., Schauble E. A. and Eiler J. M. (2004) Equilibrium thermodynamics of multiply substituted isotopologues of molecular gases. *Geochim. Cosmochim. Acta* **68**, 4779–4797.

Watkins J. M., Nielsen L. C., Ryerson F. J. and DePaolo D. J. (2013) The influence of kinetics on the oxygen isotope composition of calcium carbonate. *Earth Planet. Sci. Lett.* **375**, 349–360.

Watson E. B. (2004) A conceptual model for near-surface kinetic controls on the trace-element and stable isotope composition of abiogenic calcite crystals. *Geochim. Cosmochim. Acta* **58**, 1473–1488.

Watson E. B. and Müller T. (2009) Non-equilbrium isotopic and elemental fractionation during diffusion-controlled crystal growth under static and dynamic conditions. *Chem. Geol.* **267**, 111–124.

Zaarur S., Affek H. P. and Brandon M. (2013) A revised calibration of the clumped isotope thermometer. *Earth Planet. Sci. Lett.* **382**, 47–57.

Associate editor: Edwin Schauble